J. Fluid Mech. (1986), *vol.* 169, *pp.* 353–377
Printed in Great Britain

Two-dimensional disturbance travel, growth and spreading in boundary layers

By F. T. SMITH

Department of Mathematics, University College London, Gower Street, London WC1E 6BT

(Received 4 October 1985)

The nonlinear growth of Tollmien–Schlichting disturbances in a boundary layer is considered as an initial-value problem, for the unsteady two-dimensional triple deck, and computational and analytical solutions are presented. On the analytical side, the nonlinear properties of relatively high-frequency/high-speed disturbances are discussed. The disturbances travel at the group velocity and their amplitude is controlled by a generalized cubic Schrödinger equation, during a first stage of the nonlinear development. The equation, which has been studied in other contexts also, is integrated numerically here, and the resulting large-time/far-downstream behaviour is then deduced analytically. This behaviour comprises an exponentially fast growth and spreading of the disturbance, the spreading being governed only by an integral property of the initial disturbance. Secondary sideband instability does not occur, and there is no conclusive sign of a chaotic response, during this stage, although the three-dimensional counterpart could well yield both phenomena. In the subsequent (and more nonlinear) second stage further downstream, however, where the amplitude is larger, spiked behaviour and spectrum broadening can occur because of vorticity bursts from the viscous sublayer. Computationally, two forms of numerical solution of the triple-deck problem, one spectral, the other finite-difference, are given. The results from each form tend to support the conclusions of the high-frequency analysis for initial-value problems, and recent calculations of the two-dimensional unsteady Navier–Stokes equations also provide some backing. One implication is that the unsteady planar interacting-boundary-layer equations, or a composite version, can capture much of the physics involved in the beginnings of boundary-layer transition although, again, three-dimensionality is undoubtedly an important element which will need to be incorporated eventually.

1. Introduction

Numerous experiments concerned with the major features of transition to turbulence in boundary layers have investigated the development of sizeable disturbances progressing downstream of either an initial impulse or a maintained forcing. Prime examples are the development of turbulent spots (Wygnanski, Sokolov & Friedman 1976) and the disturbed flow produced by a vibrating source or system of sources (Saric, Kozlov & Levchenko 1984; Gaster 1984; Klebanoff, Tidstrom & Sargent 1962). The travel, growth and spreading of such disturbances downstream and the subsequent transition of the boundary layer have remained largely beyond theoretical description for a long time, however, although large-scale computation does model certain of the observed features. The complicated practical features associated with the progress of sizeable disturbances, in time and space, provide ultimately the main motivation or goal for the present work, which is concerned with re-emphasizing the study of

initial-value problems in disturbed boundary layers. As a convenient starting point below we take two-dimensional unsteady flow since, even though in reality three-dimensionality matters greatly, the two-dimensional case can act as a useful test bed, numerically or otherwise, for many of the theoretical predictions involved. The current work then has two principal aspects to it, one analytical and one computational, with both aspects addressing the nonlinear unsteady triple-deck problem. As is shown by Smith (1979*a*, *b*) and Smith & Burggraf (1985, hereinafter referred to as SB) this nonlinear viscous–inviscid problem governs the important first stages in the nonlinear development of Tollmien–Schlichting disturbances in an attached boundary layer. Emphasis is given below to the analytical aspects, concerning in particular the formation of high-frequency high-speed nonlinear disturbances from an initial state. The computational aspect, again for initial-value problems, is described in Appendix B.

The initial-value problem for a boundary layer, as governed by the triple deck at high Reynolds numbers Re, is significant especially for its predictions of the behaviour downstream of the initial disturbance. The problem is a difficult one generally, however, because the maximum growth rate of infinitesimal disturbances is not relatively small and so, in contrast to some other contexts, an assumption of weak growth, coupled with weak nonlinearity and slow modulation, is not valid in general. A global nonlinear initial-value problem for an arbitrary initial disturbance is instead necessarily a full nonlinear, and hence computational, problem (see Appendix B). Again, strictly one cannot turn to the option, available for parallel-channel-flow studies (Stewartson & Stuart 1971; Hocking & Stewartson 1972) for instance, of investigating the weak growth which occurs at a finite critical Reynolds number, because at finite Reynolds numbers the basic boundary layer is a fully nonparallel entity, a fact which strictly rules out the existence of a unique critical Reynolds number anyway (Smith 1979*a*, although numerically the parallel-flow approximation turns out to work reasonably well in practice). The approach we adopt analytically in the present study, therefore, partly to compare with the fully computational aspect, is to regard the initial disturbance as a nonlinear packet of relatively high-frequency waves. With that restriction, the growth rate *is* relatively small and the slow nonlinear modulation of the wave packet can be analysed as the packet travels downstream, at the (real) group velocity, from its starting state upstream. The susceptibility of such a travelling disturbance to a Benjamin–Feir sideband instability, conjectured by Gaster (1984), can also be examined then. The relatively high-frequency regime, which is studied mainly in an attempt to gain more theoretical insight into the crucial nonlinear initial-value problem, does exhibit a number of intriguing properties of its own. These nonlinear properties could be quite significant in practice, since the high-frequency part of an initial disturbance travels the fastest, having such short lengthscales that the group velocity is relatively large. Moreover, it is found that the corresponding amplitude increase remains unsuppressed nonlinearly for a large distance downstream, whereas some lower-frequency nonlinear disturbances soon stabilize by attaining an equilibrium amplitude (see Smith 1979*b* and SB).

The unsteady planar subsonic boundary layer is considered locally here, this being equivalent to the incompressible case in view of a Prandtl–Glauert transformation; we note that the supersonic counterpart, in contrast, is stable except for relatively long waves (Ryzhov & Zhuk 1980; Duck 1985). The central unsteady triple-deck problem of concern (§2) deals with scaled values of the velocity $U_D(u, v)$, the Cartesian coordinates $l_D(x, y)$, the pressure variation $\rho_D U_D^2 p$ and the time $l_D t/U_D$, where U_D, l_D, ρ_D stand for the typical dimensional flow speed (e.g. the local free-stream value),

the lengthscale (e.g. airfoil chord) and the fluid density respectively. The basic boundary layer is assumed (usually) to be on a flat surface $y = 0$ locally and its nonlinear stability properties are examined near a typical station x of $O(1)$. Section 2 describes the behaviour of a relatively high-frequency, short-wavelength disturbance packet as it travels downstream, the behaviour being controlled by a generalized Schrödinger equation for the pressure, during the first stage of the nonlinear development. The timescale t here satisfies $Re^{-\frac{1}{4}} \gg t \gg Re^{-\frac{1}{2}}$ (see also SB), the pressure is relatively large and overall the disturbance size is much greater than the basic flow in the main region of interest near the surface. Section 3 then extends the analysis to nonparallel flows where, for example, there is a distortion of the solid surface present or where the basic flow is a breakaway separation. The pressure solution and the large-time/far-downstream behaviour of the disturbance are discussed in §§4 and 5. In particular, the disturbance amplitude is found to grow and spread at exponentially fast rates, with the amplitude dependence taking on an expanding *elliptical* shape whose precise size is governed by an integral property of the initial condition. The sideband instability mentioned earlier does not occur in the present context, although it cannot be ruled out for more general situations. Again, during the subsequent second stage, which occurs further downstream and is more nonlinear, bursting from the viscous sublayer can lead to spectrum broadening in addition, and other forms of spiky secondary instability are also possible. Further comments are given in §6, including comparisons with computations, while the Appendices A and B describe, in turn, certain properties of the high-frequency amplitude equation and computational time-marching solutions of the full triple-deck problem. A conclusion drawn is that the two-dimensional unsteady interacting-boundary-layer equations, or a composite version, can capture much of the physics involved in the beginnings of boundary-layer transition, although again the important element of three-dimensionality will need to be incorporated in due course.

We would add here that the high-frequency/high-speed regime considered below corresponds in effect to movement downstream of the lower branch (SB), towards the upper branch of the neutral curve based on infinitesimal-perturbation theory, for the Blasius boundary layer for example. Many of the properties found hold across the entire distance to the upper branch and beyond, thus enlarging the scope of the theory. Similar properties are expected to hold in other basic flows also. Further, this regime appears to be the second broad regime open to the analytical study of nonlinear wave packets in through flows, the first being that developed by Stewartson & Stuart (1971) and Hocking & Stewartson (1972) for near-critical properties. Unlike the latter, however, the high-frequency/high-speed regime is not restricted to (the few) parallel basic flows, and this would seem to be a considerable advantage.

2. Flow structure and governing equations

The nonlinear behaviour of amplifying Tollmien–Schlichting disturbances, in an otherwise attached boundary layer, is governed initially by the triple-deck structure. This has the short lengthscale $O(Re^{-\frac{3}{8}})$ locally in x, the critical timescale is fast, $t = O(Re^{-\frac{1}{4}})$, and the central problem of the fully nonlinear instabilities is to solve the unsteady boundary-layer equations

$$U = \frac{\partial \Psi}{\partial Y}, \quad \frac{\partial U}{\partial T} + U\frac{\partial U}{\partial X} - \frac{\partial \Psi}{\partial X}\frac{\partial U}{\partial Y} = -\frac{\partial P}{\partial X} + \frac{\partial^2 U}{\partial Y^2} \qquad (2.1\,a, b)$$

holding in the lower deck near the surface. Here $y = Re^{-\frac{1}{8}}Y$, $x = Re^{-\frac{3}{8}}X$, $t = Re^{-\frac{1}{4}}T$, $u = Re^{-\frac{1}{8}}U$, $p = Re^{-\frac{1}{4}}P(X,T)$ and Ψ is the scaled stream function. Equations (2.1*a*, *b*) follow formally from the Navier–Stokes equations, with the unknown pressure P being independent of Y. The boundary conditions appropriate for no slip at the surface and matching with the main deck are

$$U = \Psi = 0 \quad \text{at } Y = 0, \tag{2.1c}$$

$$U \sim Y + A(X,T) \quad \text{as } Y \to \infty \tag{2.1d}$$

respectively, where the function $A(X,T)$ represents the unknown decrement of the boundary-layer displacement. Finally the pressure–displacement interaction via the upper deck outside the original boundary layer requires the law

$$P(X,T) = \frac{1}{\pi} \int\!\!\!\!\!\!- _{-\infty}^{\infty} \frac{\partial A}{\partial \xi}(\xi,T) \frac{\mathrm{d}\xi}{X-\xi} \tag{2.1e}$$

to be satisfied, for incompressible fluid/subsonic flow, with the bar denoting the principal value of the Cauchy–Hilbert integral.

The context of the problem (2.1 *a–e*) for boundary-layer instability is described by Smith (1979*a*, *b*) and in the related paper SB. Here we need note only that the traditional skin-friction factor $\lambda(x)$ has already been scaled out, and that the properties of (2.1 *a–e*) are of concern for all values of the reduced fundamental frequency $\Omega = O(|\partial/\partial T|)$. As the above references observe, an increase in the value of Ω results either from a downstream movement of our observation position x or from an increase in the fundamental frequency of the disturbances present. In particular the basic steady flow, $U = Y$, $P = A \equiv 0$, is linearly unstable/stable for $\Omega \gtrless \Omega_c$, where $\Omega_c \doteq 2.30$, and a stable supercritical bifurcation occurs for Ω just exceeding Ω_c. Our concern however is with the high-frequency supercritical properties (see figure 1) where Ω is large, as in SB. In SB it is shown that an initially small disturbance for Ω large goes through two stages, 1 and 2, as the disturbance amplifies. Stage 1 is controlled by a weakly nonlinear modulation which, somewhat unusually, affects the phase but not the amplitude of the exponentially growing disturbance. In the subsequent stage 2 stronger nonlinearity then comes into play, leading to the Benjamin–Ono equation for the displacement: see further comments in §6. The present paper re-addresses stage 1, in view of the following feature. When Ω is large any disturbance, although unstable, has only a relatively small growth rate, and to leading order the corresponding spatial wavenumber α is real and large, being given by

$$\alpha = \Omega^{\frac{1}{2}} + O(\Omega^{-\frac{1}{2}}), \tag{2.2}$$

from the dispersion relation of linear theory (SB, equation (2.5)). Hence the group velocity $c_g \propto \mathrm{d}\Omega/\mathrm{d}\alpha$ is real then, to leading order. In consequence a packet of waves travelling at the group velocity can be considered, with their small growth being balanced by their nonlinearity and by the relative dispersion in the streamwise direction. This in turn allows an initial-value problem to be posed, starting from an initially bounded state, as seems preferable on physical grounds.

We reconsider stage 1 of the high-frequency short-scaled disturbances, therefore. As in SB the flow solution expands in the form

$$\Psi = \Omega^{-\frac{1}{2}} \psi_0 + \Omega^{-1} \psi_1 + \Omega^{-\frac{3}{2}} \psi_2 + \ldots, \tag{2.3a}$$

$$U = u_0 + \Omega^{-\frac{1}{2}} u_1 + \Omega^{-1} u_2 + \ldots, \tag{2.3b}$$

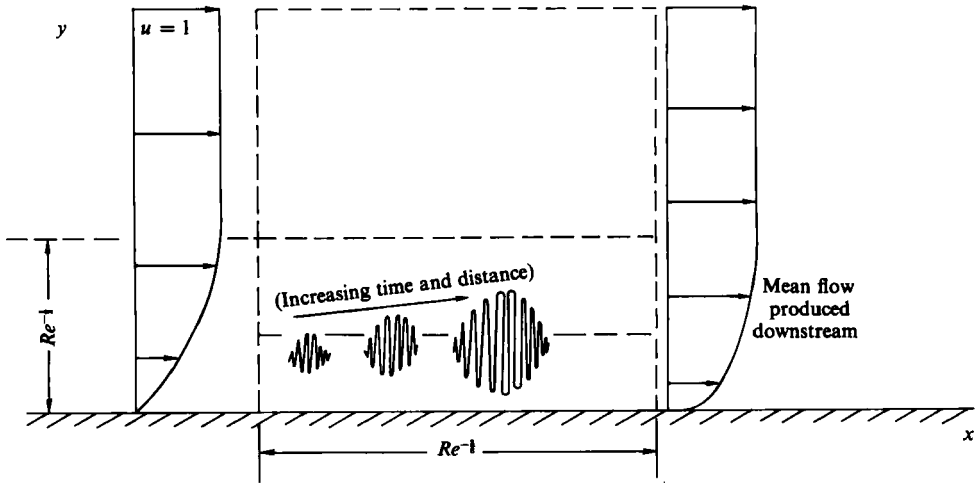

FIGURE 1. Schematic diagram (not to scale) of the travel, nonlinear growth and spreading of a relatively high-frequency Tollmien–Schlichting disturbance introduced into the boundary layer, according to the triple-deck structure. See §2.

in a Stokes sublayer where $Y = \Omega^{-\frac{1}{2}} z$ is small. The pressure and negative displacement have the corresponding developments

$$P = \Omega^{\frac{1}{2}} p_0 + p_1 + \Omega^{-\frac{1}{2}} p_2 + \ldots, \tag{2.3c}$$

$$A = A_0 + \Omega^{-\frac{1}{2}} A_1 + \Omega^{-1} A_2 + \ldots. \tag{2.3d}$$

Unlike in SB, however, the temporal and spatial dependences are both now considered to be of the multi-scaled type, with

$$\frac{\partial}{\partial T} \to \Omega \frac{\partial}{\partial T_0} + \Omega^{\frac{1}{2}} \frac{\partial}{\partial T_1} + \frac{\partial}{\partial T_2} + \ldots, \tag{2.4a}$$

$$\frac{\partial}{\partial X} \to \Omega^{\frac{1}{2}} \frac{\partial}{\partial X_0} + \frac{\partial}{\partial X_1} + \Omega^{-\frac{1}{2}} \frac{\partial}{\partial X_2} + \ldots. \tag{2.4b}$$

In addition, the extra intermediate variables X_1, T_1 are introduced here. The relative slowness of the T_1, T_2, ... and X_1, X_2 ... derivatives is implied by the known relation (2.2) combined with the relative nonlinear effects, as in SB. The successive governing equations resulting from formal substitution of (2.3*a–d*), (2.4*a*, *b*) into (2.1*a*, *b*) are then

$$u_0 = \frac{\partial \psi_0}{\partial z}, \quad \frac{\partial u_0}{\partial T_0} = -\frac{\partial p_0}{\partial X_0} + \frac{\partial^2 u_0}{\partial z^2}, \tag{2.5a, b}$$

$$u_1 = \frac{\partial \psi_1}{\partial z}, \quad \frac{\partial u_1}{\partial T_0} + \frac{\partial u_0}{\partial T_1} + \left(u_0 \frac{\partial u_0}{\partial X_0} - \frac{\partial \psi_0}{\partial X_0} \frac{\partial u_0}{\partial z} \right) = -\frac{\partial p_1}{\partial X_0} - \frac{\partial p_0}{\partial X_1} + \frac{\partial^2 u_1}{\partial z^2}, \tag{2.6a, b}$$

$$u_2 = \frac{\partial \psi_2}{\partial z}, \tag{2.7a}$$

$$\frac{\partial u_2}{\partial T_0} + \frac{\partial u_1}{\partial T_1} + \frac{\partial u_0}{\partial T_2} + \left(u_0 \frac{\partial u_0}{\partial X_1} + u_0 \frac{\partial u_1}{\partial X_0} + u_1 \frac{\partial u_0}{\partial X_0} - \frac{\partial \psi_0}{\partial X_1} \frac{\partial u_0}{\partial z} - \frac{\partial \psi_1}{\partial X_0} \frac{\partial u_0}{\partial z} - \frac{\partial \psi_0}{\partial X_0} \frac{\partial u_1}{\partial z} \right) = \frac{\partial p_2}{\partial X_0} - \frac{\partial p_1}{\partial X_1} - \frac{\partial p_0}{\partial X_2} + \frac{\partial^2 u_2}{\partial z^2}. \tag{2.7b}$$

The nonlinear contributions are enclosed in the brackets in (2.6b) and (2.7b). The boundary conditions on the sets of unknown functions (ψ_0, u_0, p_0, A_0), (ψ_1, u_1, p_1, A_1), (ψ_2, u_2, p_2, A_2) above are

$$u_n = \psi_n = 0 \text{ at } z = 0 \quad (n = 0, 1, 2), \tag{2.8a}$$

$$u_0 \to A_0,\ u_1 \sim z + A_1,\ u_2 \to A_2 \quad \text{as } z \to \infty, \tag{2.8b}$$

from (2.1c, d), while the pressure-displacement law (2.1e) gives

$$p_0 = \frac{1}{\pi}\int_{-\infty}^{\infty} \frac{\partial A_0}{\partial \xi_0}(\xi_0, X_1, X_2, \ldots, T_0, T_1, T_2)\frac{\mathrm{d}\xi_0}{(X_0 - \xi_0)}, \tag{2.8c}$$

$$p_1 = \frac{1}{\pi}\int_{-\infty}^{\infty} \left(\frac{\partial A_1}{\partial \xi_0} + \frac{\partial A_0}{\partial X_1}\right)\frac{\mathrm{d}\xi_0}{(X_0 - \xi_0)}, \tag{2.8d}$$

$$p_2 = \frac{1}{\pi}\int_{-\infty}^{\infty} \left(\frac{\partial A_2}{\partial \xi_0} + \frac{\partial A_1}{\partial X_1} + \frac{\partial A_0}{\partial X_2}\right)\frac{\mathrm{d}\xi_0}{(X_0 - \xi_0)}, \tag{2.8e}$$

in turn. It is observed that the basic velocity profile ($U = Y$) affects only the second- and higher-order terms directly, through the contribution z in u_1 in (2.8b), because in the current sublayer $|U|$ is much larger than $|Y|$.

At first order, where (2.5a, b) apply with (2.8a–c), the solution has the form

$$(\psi_0, u_0, p_0, A_0) = (\psi_{01}, u_{01}, p_{01}, A_{01})E + \text{c.c.}, \tag{2.9}$$

with c.c. denoting the complex conjugate of the preceding bracket. Here

$$E \equiv \exp(\mathrm{i}\alpha_0 X_0 - \mathrm{i}T_0), \tag{2.10}$$

the real $O(1)$ constant α_0 is to be found, and ψ_{01}, etc. are independent of X_0, T_0. From (2.5a, b), (2.8a) with (2.9) we obtain the results

$$u_{01} = \alpha_0 p_{01}(1 - \mathrm{e}^{mz}), \quad \psi_{01} = \alpha_0 p_{01}(z - m^{-1}\mathrm{e}^{mz} + m^{-1}), \tag{2.11a, b}$$

where $m \equiv \exp(\frac{3}{4}\pi\mathrm{i})$. So (2.8$b$) then yields $A_{01} = \alpha_0 p_{01}$. But from (2.8c), with (2.9), $p_{01} = |\alpha_0| A_{01}$. Hence

$$\alpha_0 = 1, \quad A_{01} = p_{01}. \tag{2.12a, b}$$

Here the result (2.12a) is in line with the linear result (2.2), as it should be. The dominant pressure term p_{01} remains an unknown function of $X_1, X_2, \ldots, T_1, T_2, \ldots$.

At second order, both nonlinearity and the basic flow profile first enter into the reckoning, through (2.6b) and (2.8b). Accordingly, higher harmonics and a mean-flow correction are generated, in addition to there being more of the fundamental disturbance. Thus

$$u_1 = (u_{12}E^2 + u_{11}E) + \text{c.c.} + u_{1\mathrm{M}} \tag{2.13}$$

and similarly for ψ_1, p_1, A_1, with the (X_0, T_0)-dependence appearing solely in E, E^2 in (2.13). The mean-flow correction $u_{1\mathrm{M}}$ inferred from (2.6a, b) is exactly as in SB, as also is the higher harmonic u_{12}, and so in particular

$$u_{1\mathrm{M}} \sim z + A_{1\mathrm{M}}, \quad u_{12} \to A_{12} \quad \text{as } z \to \infty,$$

where

$$A_{1\mathrm{M}} = 3|p_{01}|^2, \quad A_{12} = \tfrac{1}{2}p_{12} = -\tfrac{1}{2}p_{01}^2, \tag{2.14}$$

while $p_{1\mathrm{M}}$ remains arbitrary. The new effect here, the extra fundamental u_{11} in (2.13), is found to be given by

$$u_{11} = \left[p_{11} - \mathrm{i}\frac{\partial p_{01}}{\partial T_1} - \frac{\partial p_{01}}{\partial X_1}\right](1 - \mathrm{e}^{mz}) - \frac{\partial p_{01}}{\partial T_1}\frac{z}{2m}\mathrm{e}^{mz}, \tag{2.15}$$

from (2.6*b*), (2.8*a*), given (2.9), (2.11*a*)–(2.12*b*) and (2.13). Therefore in view of (2.8*b*) A_{11} is equal to the contribution in square brackets in (2.15). On the other hand, the interaction (2.8*d*) now yields

$$A_{11} = p_{11} + \mathrm{i}\frac{\partial p_{01}}{\partial X_1}. \tag{2.16a}$$

Eliminating A_{11}, then, we have the equation

$$\left(\frac{\partial}{\partial T_1} + 2\frac{\partial}{\partial X_1}\right) p_{01} = 0 \tag{2.16b}$$

controlling the variation of p_{01} on the intermediate (X_1, T_1)-scales. This implies that at the current level $p_{01} = p_{01}(\xi_1)$ is an unknown function of $\xi_1 \equiv X_1 - 2T_1$ only, in line with the amplitude of the wave packet travelling at the effective group velocity, which is $2\alpha \approx 2\Omega^{\frac{1}{2}}$ from (2.2), i.e. twice the dominant wavespeed.

The third-order balances (2.7*a*, *b*) finally yield the main amplitude equation for p_{01} since they reproduce nonlinearly the fundamental proportional to E. If u_2 is written as

$$u_2 = (u_{21} E + u_{22} E^2 + u_{23} E^3) + \text{c.c.} + u_{2\mathrm{M}}, \tag{2.17}$$

with similar expressions for ψ_2, p_2, A_2, then $u_{21}, \psi_{21}, p_{21}, A_{21}$ satisfy the equations

$$u_{21} = \frac{\partial \psi_{21}}{\partial z}, \tag{2.18a}$$

$$-\mathrm{i}u_{21} + \frac{\partial u_{11}}{\partial T_1} + \frac{\partial u_{01}}{\partial T_2} + \left(\mathrm{i}u_{01}^* u_{12} + \mathrm{i}u_{1\mathrm{M}} u_{01} - 2\mathrm{i}\psi_{12}\frac{\partial u_{01}^*}{\partial z} - \mathrm{i}\psi_{01}\frac{\partial u_{1\mathrm{M}}}{\partial z} + \mathrm{i}\psi_{01}^*\frac{\partial u_{12}}{\partial z}\right) = -\mathrm{i}p_{21} - \frac{\partial p_{11}}{\partial X_1} - \frac{\partial p_{01}}{\partial X_2} + \frac{\partial^2 u_{21}}{\partial z^2}, \tag{2.18b}$$

with the boundary conditions of no slip at $z = 0$, and

$$u_{21} \to A_{21} \quad \text{as } z \to \infty \tag{2.18c}$$

$$p_{21} = A_{21} - 2\mathrm{i}\left(\frac{\partial A_{11}}{\partial X_1} + \frac{\partial A_{01}}{\partial X_2}\right) - \frac{\partial^2 A_{01}}{\partial X_1^2}. \tag{2.18d}$$

Here in (2.18*b*) the nonlinear contributions are grouped in brackets again, while * stands for the complex conjugate, and the constraints (2.18*c*,*d*) stem from (2.8*b*,*e*) respectively. So, letting $z \to \infty$ in (2.18*b*) and then applying (2.18*c*,*d*), which eliminates the extra fundamentals p_{21}, A_{21} here, we obtain the relation

$$\frac{\partial p_{11}}{\partial T_1} + \mathrm{i}\frac{\partial^2 p_{01}}{\partial X_1 \partial T_1} + \frac{\partial p_{01}}{\partial T_2} + \mathrm{i}p_{01}^* A_{12} + \mathrm{i}p_{01} A_{1\mathrm{M}} - \frac{\mathrm{i}}{m} p_{01} = -\frac{2\partial p_{11}}{\partial X_1} - \mathrm{i}\frac{\partial^2 p_{01}}{\partial X_1^2} - \frac{2\partial p_{01}}{\partial X_2} \tag{2.19}$$

on use also of the previous results derived at first and second order. In (2.19) the contributions involving $A_{1\mathrm{M}}$ and A_{12} mark the influences of the second-order Stokes steady streaming and second harmonics and they alone induce the nonlinear effects present. The other contributions are all higher-order linear responses in essence.

The correction p_{11} of the fundamental may be taken to vary with the group velocity, i.e. to depend only on $\xi_1 = X_1 - 2T_1$ at this level. Hence, upon substitution for A_{12}, $A_{1\mathrm{M}}$ from (2.14), the relation (2.19) becomes a generalized cubic Schrödinger equation governing p_{01},

$$\frac{\partial p_{01}}{\partial T_2} - \mathrm{i}\frac{\partial^2 p_{01}}{\partial X_1^2} = \left(\frac{1-\mathrm{i}}{\sqrt{2}}\right) p_{01} - \frac{5\mathrm{i}}{2} p_{01} |p_{01}|^2. \tag{2.20}$$

Here, on the left-hand side, the temporal derivative holds with the coordinate $\xi_2 = X_2 - 2T_2$ kept fixed, corresponding again to movement of the wave packet with the scaled group velocity of 2, while (2.16*b*) has been used to produce the double spatial derivative appearing, which perhaps more properly is $\partial^2 p_{01}/\partial\xi_1^2$. On the right-hand side, the first term provokes the linearized growth expected of the present supercritical disturbances; it is in agreement with the linear dispersion relation (Tietjens function) for high frequencies and it represents a viscous effect of the Stokes sublayer, as distinct from the main wave in (2.10), which is an inviscid feature. The second term on the right-hand side of (2.20) is the nonlinear influence. Its most significant aspect is that its coefficient, the Stuart–Landau constant $-\frac{1}{2}\mathrm{i}$, is purely imaginary. This means that in the context of SB, where the possible spreading due to the X_1 scale is ignored in (2.20) (and $\partial/\partial T_2$ is replaced by $-2\partial/\partial X_2$, so that spatial development is then under consideration), the nonlinearity has no effect on the amplitude $|p_{01}|$, which therefore continues to grow exponentially just as in linear theory: see also §5 below and Benney & Maslowe (1975). The lack of either suppression or enhancement of the amplitude growth by the nonlinear forces proportional to $p_{01}|p_{01}|^2$, combined now with the extra spatial dependence or spreading effect proportional to $\partial^2 p_{01}/\partial X_1^2$ due to the real group velocity present, makes the integration of (2.20) for the dominant unsteady pressure response p_{01} rather interesting. The double spatial derivative also allows an initial-value problem for p_{01} and subsequent evolution in time T_2 to be more properly examined than in SB, with now a compact disturbance present satisfying $|p_{01}| \to 0$ as $|X_1| \to \infty$. Similar equations are derived and/or studied by Stewartson & Stuart (1971), Hocking & Stewartson (1972) and Benney & Maslowe (1975) for the evolution of wave packets in other through flows. Complete descriptions for cases such as (2.20), however, with purely imaginary coefficients in the second and fourth terms, and with spatial non-periodicity, do not appear to have been given previously in the literature: see also §6 and Appendix A. The main properties of (2.20) for the initial-value problem are discussed in §§4, 5.

3. Non-parallel flows

The above arguments can be extended to include certain interesting flows which when undisturbed are nonparallel on the short triple-deck scale X_1, as happens for instance in breakaway separation, trailing-edge flow and flow over surface-mounted humps. This is in contrast to the relatively passive non-parallelism of the Blasius boundary layer, for example, on the longer x-scale. The influences of the short-scale non-parallelism are considered in SB and some of the working can be brought forward from that reference, although here we put a different interpretation on the resulting properties: see also Smith (1985).

The flow of concern now is governed by (2.1*a–e*) again but with, say,

$$U \sim Y + A(X,T) + F(X) \quad \text{as } Y \to \infty \tag{3.1}$$

replacing (2.1*d*) for a reduced hump shape $F(X)$. A steady-state motion therefore has U, Ψ, p, A depending non-trivially on both X and Y, examples of such motions being given in the reviews by Messiter (1983) and Smith (1986). One effect of this, in the unsteady high-frequency case considered in §2, is to add a term $-\mathrm{i}\overline{A}(X_1)p_{01}$ to the right-hand side of (2.16*b*), thus yielding the result

$$p_{01} = q_{01}(\xi_1)\exp[-\tfrac{1}{2}\mathrm{i}\textstyle\int \overline{A}(X_1)\,\mathrm{d}X_1], \tag{3.2}$$

since the X_1 scale coincides with X. Here q_{01} is an unknown function of ξ_1, while $\overline{A}$ is the steady-state solution for A, i.e. the (non-parallel) solution of (2.1*a–c*, *e*) with (3.1) and $\partial/\partial T \equiv 0$, but with F absorbed into $\overline{A}$ for convenience. So the phase, but not the amplitude, of the dominant pressure coefficient p_{01} now depends on the fixed coordinate X_1 as well as on the moving one $\xi_1 = (X_1 - 2T_1)$. Second, the mean flow in the zone where Y is $O(1)$ is still found to satisfy the steady-state problem, which fixes $\overline{A}$, $\overline{p}$. The third effect of note comes into the amplitude equation controlling p_{01}, which now has the terms

$$\mathrm{i}\overline{A}p_{11} - \mathrm{i}p_{01}(\tfrac{5}{4}\overline{A}^2 + 2\overline{p}) + \tfrac{3}{2}p_{01}\frac{\mathrm{d}\overline{A}}{\mathrm{d}X_1} \tag{3.3}$$

added to the left-hand side of (2.19), apart from a small mean-flow correction. Here $\overline{p}$ is the steady-state solution for the pressure p. Hence, for the X_1 and $(X_1 - 2T_1)$-dependence to balance out, it follows that p_{11} must contain the contribution

$$p_{11} = -\tfrac{1}{2}[\tfrac{3}{2}\overline{A}(X_1) - \mathrm{i}\int(\tfrac{5}{4}\overline{A}^2 + 2\overline{p})\,\mathrm{d}X_1]p_{01}, \tag{3.4}$$

among others. That leaves p_{01} (or rather q_{01}) still satisfying the equation (2.20) derived earlier. The fourth main effect to record here is that the mean-flow shear stress at the wall is now $\lambda(X_1) + 2^{\frac{1}{2}}|p_{01}|^2$ (in scaled terms), where $\lambda(X_1)$ is the reduced skin friction associated with the steady-state flow solution.

The above serves to reinforce the value of solving (2.20), a matter discussed in the next two sections. However, (3.4) shows that the non-parallelism present can still have some impact, for whereas the dominant pressure amplitude $|p_{01}|$ is uniform on the intermediate X_1 scale (see (3.2)) the main correction–pressure amplitude $|p_{11}|$ is not, in general. Thus the question of whether small-amplitude growth or decay occurs on the fixed X_1 scale is decided primarily by (3.4), i.e. by the local pressure and displacement. If these effects ever become sufficiently large, then the growth or decay associated with (3.4) can become a leading-order influence: see also §6 below. Another type of non-parallel-flow effect, corresponding to trailing-edge motions in particular, should also be mentioned here. The analysis in §2 continues to apply in the interactive part of the wake of a flat plate, or thin airfoil, provided account is taken of the continuous-stress condition replacing the no-slip constraint there. This alteration leads to the coefficient of the p_{01} term in (2.20) being replaced by zero in the wake part of the flow field. So, as the governing equation (2.20) holds in the moving frame of $\xi_1 = (X_1 - 2T_1)$ kept fixed, the result is that if the disturbance p_{01} starts off upstream of the trailing edge it is controlled at first by (2.20) but then, as it progresses downstream, the linear-growth coefficient (of p_{01}) becomes equal to zero, since $\xi_1 > -2T_1$ in effect. This therefore has a stabilizing effect on the disturbance amplitude as the disturbance passes the trailing edge. A further extension of the analysis can be made, and is currently being considered, to include the influence of a basic unsteady motion, e.g. due to an oscillatory hump, although then the extra unsteady forcing has relatively little effect unless it is of high frequency. For the $O(1)$ time (T_2)-derivative in (2.4*a*) is of relative order Ω^{-1} and so any basic T_2 dependence first appears actively at the third order, affecting only the phase of the correction pressure p_{11}, not its amplitude. In consequence a basic-flow dependence on the timescale T_2, as at an oscillating trailing edge for instance, is a quasi-steady affair represented primarily by the X_1 dependence in the basic $A(X_1, T_2)$ and $p(X_1, T_2)$ functions, so far as the amplitude response of high-frequency disturbances is concerned.

4. Numerical method and results

As far as the author is aware, the nonlinear Schrödinger equation (2.20) for the pressure is not (yet) solvable by inverse-scattering techniques, and in any case there seems to be a general acknowledgement that direct numerical integration is perhaps more appropriate for obtaining explicit results from such equations. We performed the necessary numerical work for (2.20) as follows, after setting

$$p_{01} = (\tfrac{2}{5})^{\frac{1}{2}} \exp\left(\frac{-\mathrm{i}T_2}{\sqrt{2}}\right) B(X_1, T_2) \tag{4.1}$$

to convert (2.20) to the form

$$\mathrm{i}\frac{\partial B}{\partial T_2} + \frac{\partial^2 B}{\partial X_1^2} - \frac{\mathrm{i}}{\sqrt{2}} B - B|B|^2 = 0 \tag{4.2}$$

for $B(X_1, T_2)$. The boundary conditions here are $|B| \to 0$ as $X_1 \to \pm\infty$ and the initial distribution $B(X_1, 0)$ is assumed known.

Then if $B = C + \mathrm{i}D$, where C and D are real, the complex equation (4.2) may be split conveniently into four real first-order equations,

$$\hat{C} = \frac{\partial C}{\partial X_1}, \quad \hat{D} = \frac{\partial D}{\partial X_1}, \tag{4.3a, b}$$

$$\frac{-\partial D}{\partial T_2} + \frac{\partial \hat{C}}{\partial X_1} + \frac{1}{\sqrt{2}} D - (C^2 + D^2) C = 0, \tag{4.3c}$$

$$\frac{\partial C}{\partial T_2} + \frac{\partial \hat{D}}{\partial X_1} - \frac{1}{\sqrt{2}} C - (C^2 + D^2) D = 0, \tag{4.3d}$$

for C, D, $\hat{C}$, $\hat{D}$. These may be discretized in a fairly standard finite-difference form, with second-order accuracy in time and space, on a uniform grid $X_1 = X_{-\infty} + (\mathrm{i}-1)\Delta = X_{1i}$, for $i = 1$ to I, with small mesh size Δ in X_1 and with a uniform small timestep δ in T_2. Here the end points $X_{-\infty}$ and $X_{+\infty} = X_{-\infty} + (I-1)\Delta$ are suitably large and negative/positive respectively. If the subscript i denotes an unknown function value at $X_1 = X_{1i}$ and the superscripts (o), (n) stand for evaluation at the successive time levels $T_2 - \delta$, T_2, then the numerical approximations used for (4.3a–d) are, for $i = 2$ to I,

$$\tfrac{1}{2}[\hat{C}_i^{(\mathrm{a})} + \hat{C}_{i-1}^{(\mathrm{a})}] = \frac{C_i^{(\mathrm{a})} - C_{i-1}^{(\mathrm{a})}}{\Delta}, \tag{4.4a}$$

$$\tfrac{1}{2}[\hat{D}_i^{(\mathrm{a})} + \hat{D}_{i-1}^{(\mathrm{a})}] = \frac{D_i^{(\mathrm{a})} - D_{i-1}^{(\mathrm{a})}}{\Delta}, \tag{4.4b}$$

$$-\frac{D_i^{(\mathrm{n})} + D_{i-1}^{(\mathrm{n})} - D_i^{(\mathrm{o})} - D_{i-1}^{(\mathrm{o})}}{2\delta} + \frac{\hat{C}_i^{(\mathrm{a})} - \hat{C}_{i-1}^{(\mathrm{a})}}{\Delta}$$
$$+ 8^{-\frac{1}{2}}[D_i^{(\mathrm{a})} + D_{i-1}^{(\mathrm{a})}] - \tfrac{1}{8}[(C_i^{(\mathrm{a})} + C_{i-1}^{(\mathrm{a})})^2 + (D_i^{(\mathrm{a})} + D_{i-1}^{(\mathrm{a})})^2][C_i^{(\mathrm{a})} + C_{i-1}^{(\mathrm{a})}] = 0, \tag{4.4c}$$

$$\frac{C_i^{(\mathrm{n})} + C_{i-1}^{(\mathrm{n})} - C_i^{(\mathrm{o})} - C_{i-1}^{(\mathrm{o})}}{2\delta} + \frac{\hat{D}_i^{(\mathrm{a})} - \hat{D}_{i-1}^{(\mathrm{a})}}{\Delta}$$
$$- 8^{-\frac{1}{2}}[C_i^{(\mathrm{a})} + C_{i-1}^{(\mathrm{a})}] - \tfrac{1}{8}[(C_i^{(\mathrm{a})} + C_{i-1}^{(\mathrm{a})})^2 + (D_i^{(\mathrm{a})} + D_{i-1}^{(\mathrm{a})})^2][D_i^{(\mathrm{a})} + D_{i-1}^{(\mathrm{a})}] = 0, \tag{4.4d}$$

where $Z^{(\mathrm{a})}$ is the unknown average value $\frac{1}{2}[Z^{(\mathrm{n})} + Z^{(\mathrm{o})}]$ for any quantity Z. So, with the (o) values known, (4.4a–c) combined with the end conditions

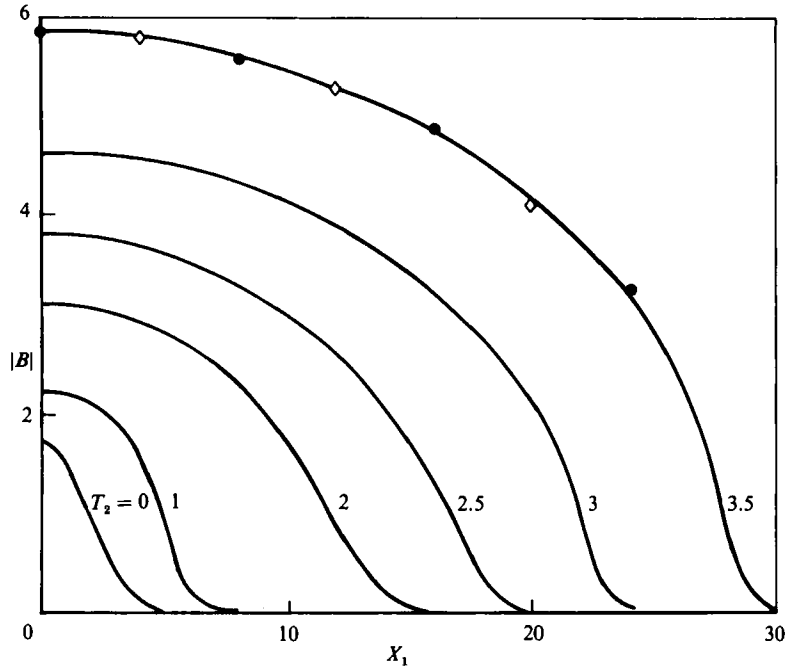

FIGURE 2. The computed amplitude $|B|$ versus X_1, at various times T_2, from §4. Initial distribution symmetric, $B = \sqrt{3}\exp(-\frac{1}{6}X_1^2)$. Symbols ◇, ● show the effects of halving $X_{\pm\infty}$ (with Δ, δ fixed) and of halving Δ, δ (with $X_{\pm\infty}$ fixed) respectively.

$C_1^{(n)} = D_1^{(n)} = C_I^{(n)} = D_I^{(n)} = 0$ provide the necessary $4I$ nonlinear equations for the $4I$ unknown (n) values at the next time level. The nonlinearity of these $4I$ equations is treated by a Newton iteration procedure which is repeated until all successive iterates differ in magnitude by less than q. Typically $q = 10^{-7}$. The matrix inversion associated with each Newton iteration here is accomplished primarily by Gaussian elimination. Given the initial distribution $B(X_1, 0)$, and hence $C, D, \hat{C}, \hat{D}$ initially, then, the calculations can be advanced forwards in timesteps δ. The typical value taken for δ was 0.001 for an X_1 grid having $I = 121$, $\Delta = 0.2$, but checks on the effects of mesh sizes were made, and these are described below.

Representative solutions are presented in figures 2 and 3. In the former example an initial distribution symmetric about $X_1 = 0$ was set and the calculations were performed first for $0 \leqslant X_1 \leqslant X_\infty$, with symmetry imposed at $X_1 = 0$ for all $T_2 > 0$, and second for $X_{-\infty} \leqslant X \leqslant X_\infty$ without the symmetry condition. The two sets of results obtained were virtually identical over the time range T_2 investigated. In the example of figure 3 no symmetry is present. Both figures also show checks on the influences of the temporal and spatial mesh sizes chosen. The checks suggest that sufficient numerical accuracy is maintained up to values of T_2 which are not too large. Another test applied concerned mainly the representation of $\pm\infty$ by $X_{\pm\infty}$ in turn and is worth mentioning here. We transformed to a stretched working coordinate $\overline{X}_1$ defined by $X_1 = \overline{X}_1/(1-\overline{X}_1)$, so that $0 \leqslant \overline{X}_1 \leqslant 1$ corresponds formally to the entire domain $X_1 \geqslant 0$, and we considered the cases symmetric about $X_1 = 0$. With uniform steps in $\overline{X}_1$ now, from $\overline{X}_1 = 0$ to $\overline{X}_1 = 1$, it was found that the numerical solutions so derived agreed very closely with the previous ones in the bulk of the original domain of interest $0 \leqslant X_1 \leqslant X_\infty$ for a fairly large range of time T_2: see also §6 below. This tends to support further the evidence of the tests shown in the figures. The

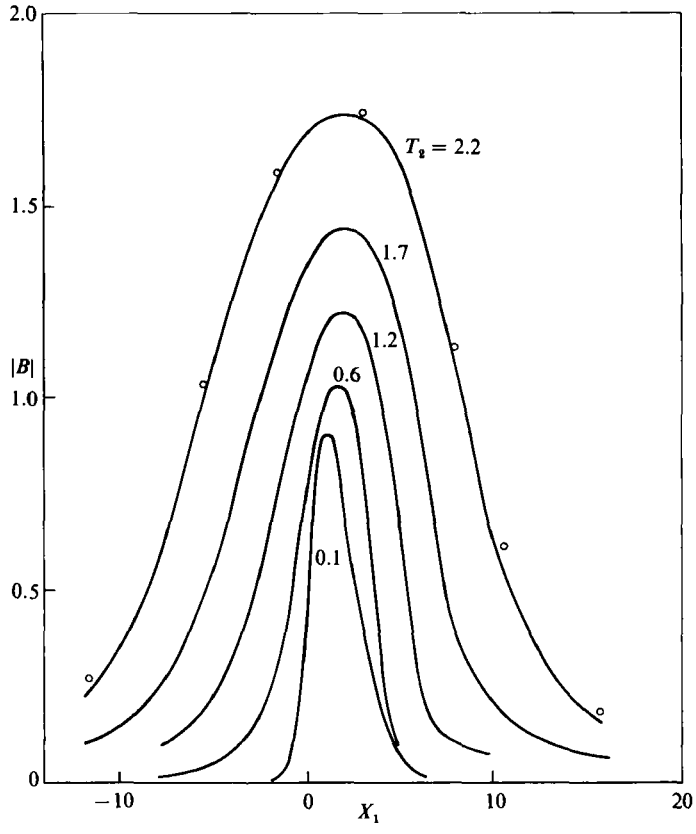

FIGURE 3. Numerical solution for the amplitude $|B|$ versus X_1, at various T_2, for the nonsymmetric initial form $B = \exp(3X_1 - \frac{1}{2}X_1^2)/[1+\exp(3X_1)]$. Symbol ○ shows the effect of halving Δ, δ with $X_{\pm\infty}$ kept fixed. A slight 'flop' in the solution is noticeable at early times.

calculations were continued to times larger than those shown in the figures but the effects from grid sizes and/or the end values $X_{\pm\infty}$ became more pronounced then.

Although the numerical studies cannot be exhaustive of course, the suggested trend, from the above results and other calculations done by the author, is one of spreading and growth of the disturbance amplitude as time T_2 goes on. That leads on to the analysis in the next section concerning the properties of the solution for larger times T_2.

5. Properties for large time/far downstream

The solution of (2.20) or (4.2) is believed to take on a limiting form with an increasingly wide spread in X_1 and large amplitude as $T_2 \to \infty$, i.e. for large times and far downstream in terms of the coordinate X_2, since ξ_2 is kept fixed above. This large-time behaviour is described below.

First, for convenience, we set $B = \exp(\gamma T_2) R \exp(i\theta)$ where γ is a real $O(1)$ constant to be specified later and R, θ are real functions of X_1, T_2. Then (4.2) yields the two real equations

$$-R\frac{\partial\theta}{\partial T_2} - R\left(\frac{\partial\theta}{\partial X_1}\right)^2 + \frac{\partial^2 R}{\partial X_1^2} - e^{2\gamma T_2}R^3 = 0, \tag{5.1a}$$

$$\left(\gamma - \frac{1}{\sqrt{2}}\right)R + \frac{\partial R}{\partial T_2} + 2\frac{\partial\theta}{\partial X_1}\frac{\partial R}{\partial X_1} + R\frac{\partial^2\theta}{\partial X_1^2} = 0, \tag{5.1b}$$

for R, θ. It is observed here, for subsequent comparison, that for the plane wave considered in SB the solution of (5.1*a*, *b*) simply has $\partial/\partial X_1 \equiv 0$ and

$$\gamma = \tfrac{1}{2}\sqrt{2}, \quad R = \text{constant}, \quad \theta = -\frac{R^2}{2\gamma}\mathrm{e}^{2\gamma T_2} + \text{constant}, \tag{5.2}$$

so that the amplitude $|B|$ grows like $\exp(T_2/\sqrt{2})$ then for all time T_2. For the evolution problem of current concern, i.e. (5.1*a*, *b*) with $R \to 0$ as $|X_1| \to \infty$, an argument based on orders of magnitude also suggests an exponentially growing amplitude for larger T_2 but accompanied by an exponential spreading in terms of the spatial coordinate X_1. Thus as $T_2 \to \infty$ we propose that

$$R = \gamma R_0(\eta) + \ldots, \quad \theta = \gamma\,\mathrm{e}^{2\gamma T_2}\phi(\eta) + \ldots, \tag{5.3}$$

where $X_1 = \mathrm{e}^{\gamma T_2}\eta$ and R_0, ϕ, η are generally $O(1)$, while γ is assumed to be positive and controls the amplitude growth $|B| \propto \exp(\gamma T_2)$. Substitution of (5.3) into (5.1*a*, *b*) leaves at leading order the coupled nonlinear ordinary differential equations

$$\eta\phi' - 2\phi - \phi'^2 = R_0^2, \tag{5.4a}$$

$$(\beta + \phi'')\,R_0 = (\eta - 2\phi')\,R_0' \tag{5.4b}$$

for $R_0(\eta)$, $\phi(\eta)$, the prime standing for $\mathrm{d}/\mathrm{d}\eta$, and the constant $\beta \equiv (\gamma - 1/\sqrt{2})/\gamma$ is unknown. It is interesting to note that the double-derivative term $\partial^2 R/\partial X_1^2$ is the only term in (5.1*a*, *b*) not to contribute to (5.4*a*, *b*). In (5.4*a*, *b*) we require $R_0(\pm\infty) = 0$.

The determination of the constant β in (5.4*a*, *b*) is important now but this can be resolved by appeal back to (5.1*b*). Multiplication of (5.1*b*) by $R(X_1, T_2)$, followed by integration with respect to X_1 from $-\infty$ to ∞, and then integration with respect to T_2, gives the integral property

$$\int_{-\infty}^{\infty} R^2(X_1, T_2)\,\mathrm{d}X_1 = \int_{-\infty}^{\infty} R^2(X_1, 0)\,\mathrm{d}X_1 \exp[(\sqrt{2} - 2\gamma)\,T_2] \tag{5.5}$$

for all times $T_2 \geqslant 0$, with the integrals assumed to be convergent. Since the large-time form in (5.3) makes the left-hand side in (5.5) of order $\exp(\gamma T_2)$, the balance $\gamma = \sqrt{2} - 2\gamma$ is required, yielding the value

$$\gamma = \tfrac{1}{3}\sqrt{2} \tag{5.6}$$

for the growth- and spreading-rate factor γ. Also, from (5.3)–(5.6), the integral property

$$\gamma^2 \int_{-\infty}^{\infty} R_0^2(\eta)\,\mathrm{d}\eta = \int_{-\infty}^{\infty} |B(X_1, 0)|^2\,\mathrm{d}X_1 \tag{5.7}$$

holds for the large-time solution.

So from (5.6) the constant $\beta = -\frac{1}{2}$. Equation (5.4*b*) is then satisfied if $\phi' = \frac{1}{2}\eta$, or

$$\phi(\eta) = \tfrac{1}{4}(\eta^2 - \tfrac{1}{2}b), \tag{5.8a}$$

where b is an unknown constant; alternative forms of solution in which $\phi' \not\equiv \frac{1}{2}\eta$ appear to be inadmissible. Given (5.8*a*), the solution for $R_0(\eta)$ follows from (5.4*a*), which yields the elliptical shape

$$R_0(\eta) = \tfrac{1}{2}(b - \eta^2)^{\frac{1}{2}} \quad \text{for } -b^{\frac{1}{2}} < \eta < b^{\frac{1}{2}}. \tag{5.8b}$$

Here b must be positive, while

$$R_0(\eta) = 0 \quad \text{for } |\eta| > b^{\frac{1}{2}}, \tag{5.8c}$$

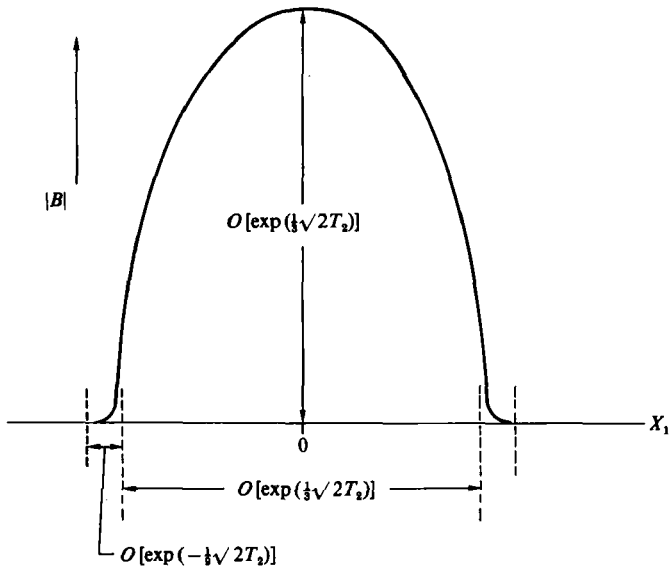

FIGURE 4. Sketch of the large-time behaviour of the effective pressure amplitude $|B|$, versus X_1, according to §5.

which again satisfies (5.4a, b) provided that $\eta\phi' = 2\phi + \gamma'^2$ for $|\eta| > b^{\frac{1}{2}}$. The relatively thin adjustment zones, required near $\eta = \pm b^{\frac{1}{2}}$ to join smoothly the solutions (5.8b, c), are considered subsequently. The constant b, however, can be determined immediately from the constraint (5.7). This gives the value

$$b = 9\left\{\tfrac{1}{2}\int_{-\infty}^{\infty} |B(X_1, 0)|^2 \, \mathrm{d}X_1\right\}^{\frac{2}{3}} \tag{5.9}$$

in terms of the initial conditions at time $T_2 = 0$.

The adjustment zones near $\eta = \pm b^{\frac{1}{2}}$ have thickness $O(\mathrm{e}^{-\frac{1}{3}\gamma T_2})$, thus bringing the highest spatial derivative $\partial^2 R/\partial X_1^2$ back into play (see figure 4). By symmetry we need consider only the adjustment zone near $\eta = b^{\frac{1}{2}}$, wherein $\tilde{\eta} = (X_1 - b^{\frac{1}{2}}\mathrm{e}^{\gamma T_2})\,\mathrm{e}^{\frac{1}{3}\gamma T_2}$ is of $O(1)$. There (5.8a–c) suggest the large-time expansions

$$R = \mathrm{e}^{-\frac{2}{3}\gamma T_2}\tilde{R}_0(\tilde{\eta}) + \mathrm{e}^{-2\gamma T_2}\tilde{R}_1(\tilde{\eta}) + \ldots, \tag{5.10a}$$

$$\theta = (\tfrac{1}{8}\gamma b)\,\mathrm{e}^{2\gamma T_2} + (\tfrac{1}{2}\gamma b^{\frac{1}{2}})\,\tilde{\eta}\,\mathrm{e}^{\frac{2}{3}\gamma T_2} + \mathrm{e}^{-\frac{2}{3}\gamma T_2}\Phi(\tilde{\eta}) + \ldots, \tag{5.10b}$$

where we postulate that ϕ, ϕ' are continuous at $\eta = b^{\frac{1}{2}}$. Substitution of (5.10a, b) into the governing equations (5.1a, b) leaves $\tilde{R}_0(\tilde{\eta})$ controlled by the nonlinear Airy equation

$$\frac{\mathrm{d}^2\tilde{R}_0}{\mathrm{d}\tilde{\eta}^2} = (\tfrac{1}{2}b^{\frac{1}{2}}\gamma^2)\,\tilde{\eta}\tilde{R}_0 + \tilde{R}_0^3. \tag{5.11a}$$

The boundary conditions here are

$$\tilde{R}_0(\tilde{\eta}) \sim \gamma(\tfrac{1}{4}b)^{\frac{1}{4}}(-\tilde{\eta})^{\frac{1}{2}} \quad \text{as } \tilde{\eta} \to -\infty, \tag{5.11b}$$

$$\tilde{R}_0(\tilde{\eta}) \to 0 \qquad\qquad \text{as } \tilde{\eta} \to \infty, \tag{5.11c}$$

the former to match with the end of the ellipse in (5.8b), while the latter is necessary for (5.8c). The controlling equation for $\Phi(\tilde{\eta})$, also from (5.1a, b), is

$$\left(-\frac{\mathrm{d}^2\Phi}{\mathrm{d}\tilde{\eta}^2} + \frac{7}{18}\sqrt{2}\right)\tilde{R}_0 = \left(2\frac{\mathrm{d}\Phi}{\mathrm{d}\tilde{\eta}} + \tfrac{1}{9}\sqrt{2}\tilde{\eta}\right)\frac{\mathrm{d}\tilde{R}_0}{\mathrm{d}\tilde{\eta}}, \tag{5.11d}$$

which can be solved, subject to the constraint $\Phi \propto \tilde{\eta}^2$ as $\tilde{\eta} \to -\infty$, consistent with (5.11*b*) and matching (5.8*a*), once $\tilde{R}_0(\tilde{\eta})$ is fixed by (5.11*a–c*). The equation (5.11*a*) however is a form of the second Painlevé transcendent, which is discussed by Hastings & McLeod (1978), who prove the existence and uniqueness of the solution to (5.11*a–c*). Hence the adjustment between (5.8*a*, *c*) near $\eta = b^{\frac{1}{2}}$ is achieved. This completes the leading-order account for the large-time far-downstream behaviour of the system (2.20) [i.e. (4.2) or (5.1*a*, *b*)] governing the flow response during stage 1 of the development of the disturbance.

6. Further discussion

The ultimate behaviour of the nonlinear disturbance packet, during the current stage 1, occurs at large times T_2 and correspondingly large distances X_2 downstream, since the disturbance travels fast at the scaled group velocity $2\Omega^{\frac{1}{2}}$. The ultimate behaviour (§5) is marked by an exponential growth in amplitude (of the pressure, displacement and so on) accompanied by an exponential rate of spatial spreading. The amplitude-growth rate here is two-thirds of the value for fully periodic disturbances, from comparison of (5.6) with (5.2), independently of the initial conditions, whereas the spreading rate is dictated by an integral property of the initial conditions, in view of (5.9). That integral property is essentially $\int_{-\infty}^{\infty} |\text{pressure}|^2 \, \mathrm{d}X$ evaluated at time $T_2 = 0$, and it is significant that this gives the sole influence of the initial disturbed conditions on the ultimate behaviour downstream. According to this, even for highly erratic initial conditions, such as the white-noise kind used experimentally by Gaster (1984) and computationally by Bretherton & Spiegel (1983), the ultimate large-time behaviour during stage 1 can be predicted by §5, as long as the flow remains planar (see later).

The computational results in §4 tend to favour qualitatively the ultimate form predicted in §5, with regard to the growths of both the amplitude and the spreading as time T_2 increases. Quantitatively, approximate values of the ratio $[\partial |B|/\partial T_1]/|B|$ evaluated at $X_1 = 0$ in figure 3 for instance are 0.33 for time $T_2 = 1.45$ and 0.38 for $T_2 = 1.95$, which are not inconsistent with the limiting value of $\frac{1}{3}\sqrt{2}[\doteq 0.4714]$ proposed in §5. Even firmer comparisons are rather hindered by the difficulties in continuing the computations to larger times without significant effects (including wave reflections from $X_{\pm\infty}$) coming into play due to the finite grid dimensions. The influence of the end values $X_{\pm\infty}$ was found to be particularly strong in that respect, as one would expect from the exponential spreading predicted in §5 for large times: see the following paragraph.

A few comments on certain other studies of the present evolution equations (4.2) or closely related ones are appropriate here. First, Appendix A addresses the high- and low-amplitude properties and concludes that the full equation must be considered in both cases: cf. Bretherton & Spiegel (1983) on the high-amplitude case for a slightly different Ginzburg–Landau equation. Further, it is noteworthy that, for the initial-value problem again, the effect of nonlinearity in the initially low-amplitude case is to reduce the amplitude-growth rate but greatly increase the spatial spreading rate, compared with the predictions of linear theory. Next, we observe that the large-time structure described in §5 is distinct from those of Hocking & Stewartson (1972), the current evolution equation being in effect a special example not considered in the last reference: see also Lange & Newell (1974). Finally here, various theoretical aspects of closely similar evolution problems are considered by Bretherton & Spiegel (1983), Kuramoto (1978), Moon, Huerre & Redekopp (1982), Bullough, Fordy & Manakov

(1982), Huppert & Moore (1976) and Kogelman & DiPrima (1970), some of whom indicate the formation of chaotic or disordered states. This is still a rather open question, although the spatial periodicity which is most often assumed in other studies where chaotic behaviour is found [for an exception see Nozaki & Bekki 1983] seems of much reduced relevance in the present context of boundary-layer motion. Our calculated results did appear to take on a somewhat chaotic form at larger times whenever the outer boundaries $X_{\pm\infty}$ were not sufficiently remote and so yielded significant reflections, but there was no firm evidence of disorder otherwise in stage 1 and, in any case, the large-time limiting structure discussed in §5 seems to be a stable though transient one (see Appendix A and Stuart & DiPrima 1978). This last comment would seem to apply also even to the ultimate effects of large and/or non-smooth initial conditions such as the white-noise kind, during the current stage 1: see however comments on the subsequent stage 2 below.

Another aspect concerns the relevance and further implications of the present high-frequency analysis. In Appendix B two computational treatments of the full triple-deck problem (2.1*a–e*) are described (see also Smith 1984; Duck 1985) for the initial-value problem, involving numerical forward marching in time T. One set of computations takes spatial periodicity in X, the other does not. Samples of the results are presented in figures 5 and 6. The set of spatially periodic results, while being rather difficult to interpret or to apply directly to the physical problems of concern, nevertheless does exhibit the predicted feature of an exponential growth in the amplitude of short-lengthscale disturbances even when nonlinearity, represented by the higher harmonics, comes into play. In addition the calculated timescale agrees well with the high-frequency theory. When spatial periodicity is not assumed, as in the second set of results, there is again good agreement with the theoretical predictions concerning the temporal and spatial scales of the main wave packet as it proceeds fairly fast downstream. Thus the high-frequency analysis is, at the least, a useful predictor of, or check against, the finite-frequency numerical properties, and the latter tend to confirm the appearance of fast-moving disturbances far downstream or at later times, with eventually some irregular behaviour setting in then: see also the subsequent remarks on stage 2. More than that, however, the analytical properties support, on a widened basis, most of the theoretical conclusions reached in SB. In particular, the mean of the wall-shear stress $\tau_w = \partial U/\partial Y(X, 0, T)$ is given by

$$\text{mean-}\tau_w = 1 + \sqrt{2}|p_{01}|^2 \tag{6.1}$$

during the current stage 1 and so, in view of §5, mean-τ_w rises exponentially fast, with increasing time and distance, while the temporal oscillations about the mean also increase dramatically. This is quite reminiscent of some transitional boundary-layer behaviour in practice.

Again, a stage 2 emerges subsequently as in SB, although the current initial-value problem slightly delays the onset. Stage 2 is a more nonlinear stage, where on inviscid grounds the nonlinear Benjamin–Ono equation takes effect in place of (2.12*a*), but subject to eruptions of vorticity or 'spikes' from a viscous sublayer which is the nonlinear extension of the Stokes sublayer and, as in stage 1, the disturbance size is much greater than that of the basic flow. This stage 2 has some connections with the work of Gatski (1983), Walker & Abbott (1977) and Walker & Scharnhorst (1977). Higher-order properties bring in spatial modulation akin to that studied in the present paper. Still higher frequencies, or shortened lengthscales, lead on to the Euler equations holding across the entire boundary layer, with vorticity emissions/spikes then also coming from the viscous wall layer present.

Reconsidering stage 1, we note that the present enlargement of SB's work to wave

packets relies on the fact that the scaled group velocity is real, and equal to *twice* the main wavespeed. (A similar enlargement is also possible in Gajjar & Smith's (1985) work on nonlinear critical layers.) Thus the wave packet overtakes individual travelling waves, a feature which is somewhat in line with Criminale & Kovasznay's (1962) calculations, even if the latter are for three-dimensional linear disturbances. There is some qualitative agreement also with Gaster's (1984) experimental findings of amplitude growth in the disturbed flow not too far downstream of a regularly or erratically vibrating source: compare the first paragraph of this section. We remark, incidentally, that in some wavemaker problems for water waves the operator $(\mathrm{i}\partial/T_2+\partial^2/\partial X_1^2)$ on the left-hand side of (4.2) may best be regarded instead as the operator $(2\mathrm{i}\partial/\partial X_2+\frac{1}{4}\partial^2/\partial T_1^2)$ involving only a single spatial derivative, suggesting the imposition of a single upstream constraint spatially in X_2. The physical relevance of this replacement in the boundary-layer context is doubtful because (4.2) holds in a moving frame (fixed X_1-2T_1), so that the wavemaker would also have to move to have effect. A travelling free-stream disturbance would be of interest, by contrast. More significantly, however, in Gaster's experiments, as in Saric *et al.* (1984) and Herbert (1984), three-dimensional behaviour is believed to exert a crucial influence experimentally as the disturbance amplitudes continue to rise, and for that reason a further extension of the present work to three-dimensional nonlinear developments (among other things) is very desirable. In the experiments, say for a fixed-frequency vibration upstream, broadening of the power-spectrum response is a significant factor downstream, whereas in the present two-dimensional analysis for stage 1 any broadening appears to be relatively minor (compare the comments on stage 2 in the next paragraph). For, supposing we start with an initial Gaussian distribution for the effective pressure B, in §4, then the corresponding Fourier transform is a Gaussian distribution concentrated around the main frequency Ω. However, the ensuing form downstream (§5) has the enlarged, elliptical shape of (5.8*b*) and therefore the transform becomes ($\propto$) a Bessel function, with a longish 'tail' producing some spectrum broadening, but with the power spectrum generally being more concentrated around Ω, unlike in experiments. The two-dimensional case studied here does lead to many features of interest, we feel, and it creates a useful and rational starting point, but bearing in mind the nonlinearity present it remains to be seen whether the three-dimensional version for stage 1 is merely a passive extension of this or not. A study along these lines has recently been started.

By contrast, stage 2 further downstream is likely to exhibit spiked or erratic behaviour, with spectrum broadening, even for two-dimensional flow, as noted in Appendix B, and possibly featured in figures 5(*b*)–(*d*). For, in stage 2, the viscous wall layer induced has a classical unsteady-boundary-layer form, which breaks down (SB) by causing a spiked emission of vorticity through a highly localized singularity in the layer's displacement. This irregular behaviour downstream, along with secondary instabilities of the Rayleigh kind and similar (Smith & Bodonyi 1985; Tutty & Cowley 1986), suggests a good qualitative link between the theory and the recent computational solutions of the unsteady Navier–Stokes equations, likewise confined to two dimensions, in Fasel's (1984) paper, where spikiness and spectrum broadening are found numerically in the more-downstream flow. Once solutions of the theoretical stage-2 problem are obtained, a quantitative comparison could be very illuminating. We conclude, then, that the two-dimensional unsteady interactive-boundary-layer equations or a composite form can capture much of the physics involved in the beginnings of the transition process although, on the other hand, three-dimensionality is without doubt an important element which will need to be included in due course.

A final comment concerns the non-parallel-flow effects considered in §3. These

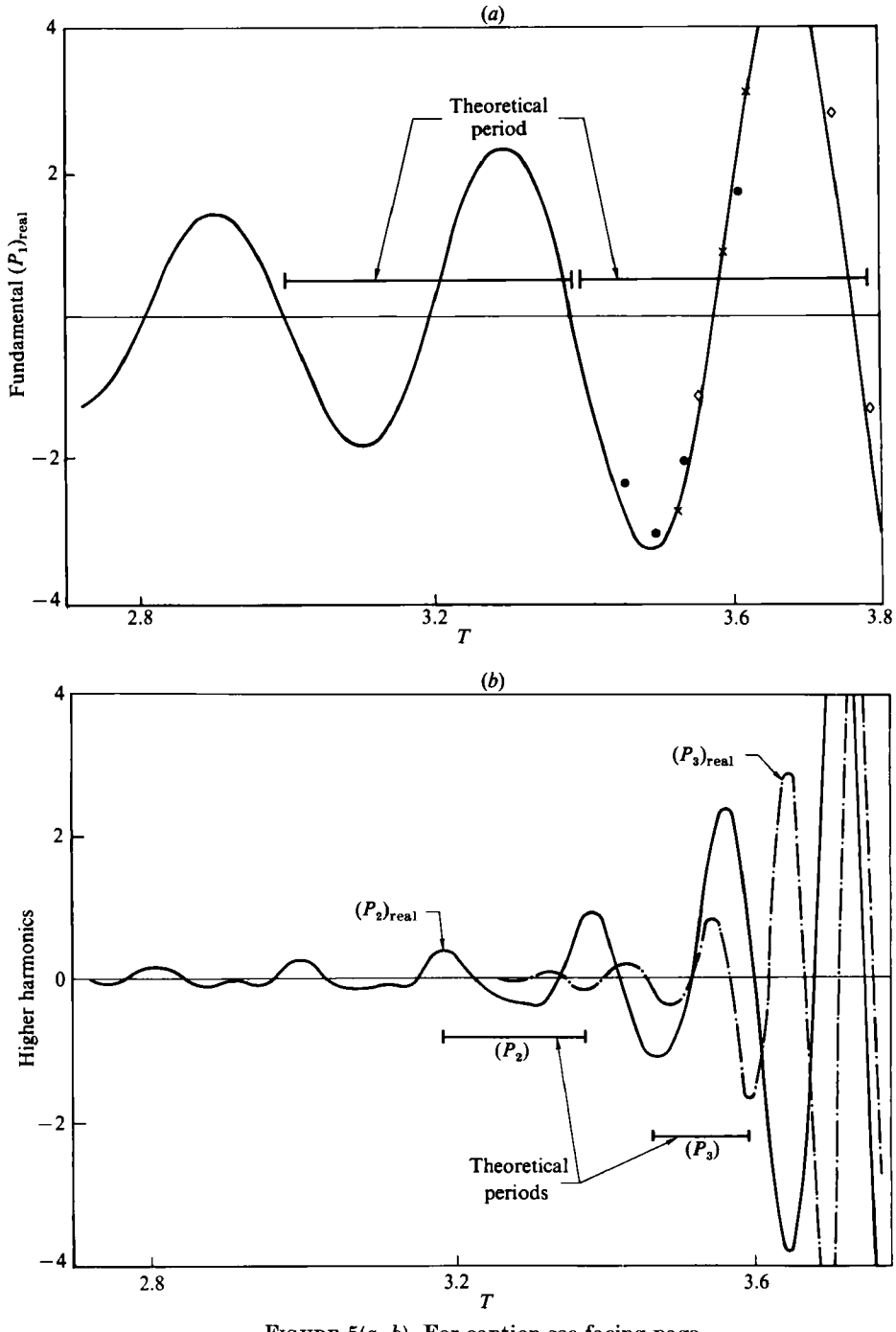

FIGURE 5(*a*, *b*). For caption see facing page.

effects can be substantial for certain flows, in view of the contribution (3.4). The net linear growth rate of disturbances, for instance, is proportional to $(\sqrt{2}-3\mathrm{d}\bar{A}/\mathrm{d}X_1)$ at leading order, and so, formally, amplitude growth can be suppressed in flows where the local displacement decrement slope $\mathrm{d}\bar{A}/\mathrm{d}X_1$ exceeds $\frac{1}{3}\sqrt{2}$, which makes sense physically, as noted in SB. Again, although the dominant pressure p_{01} grows

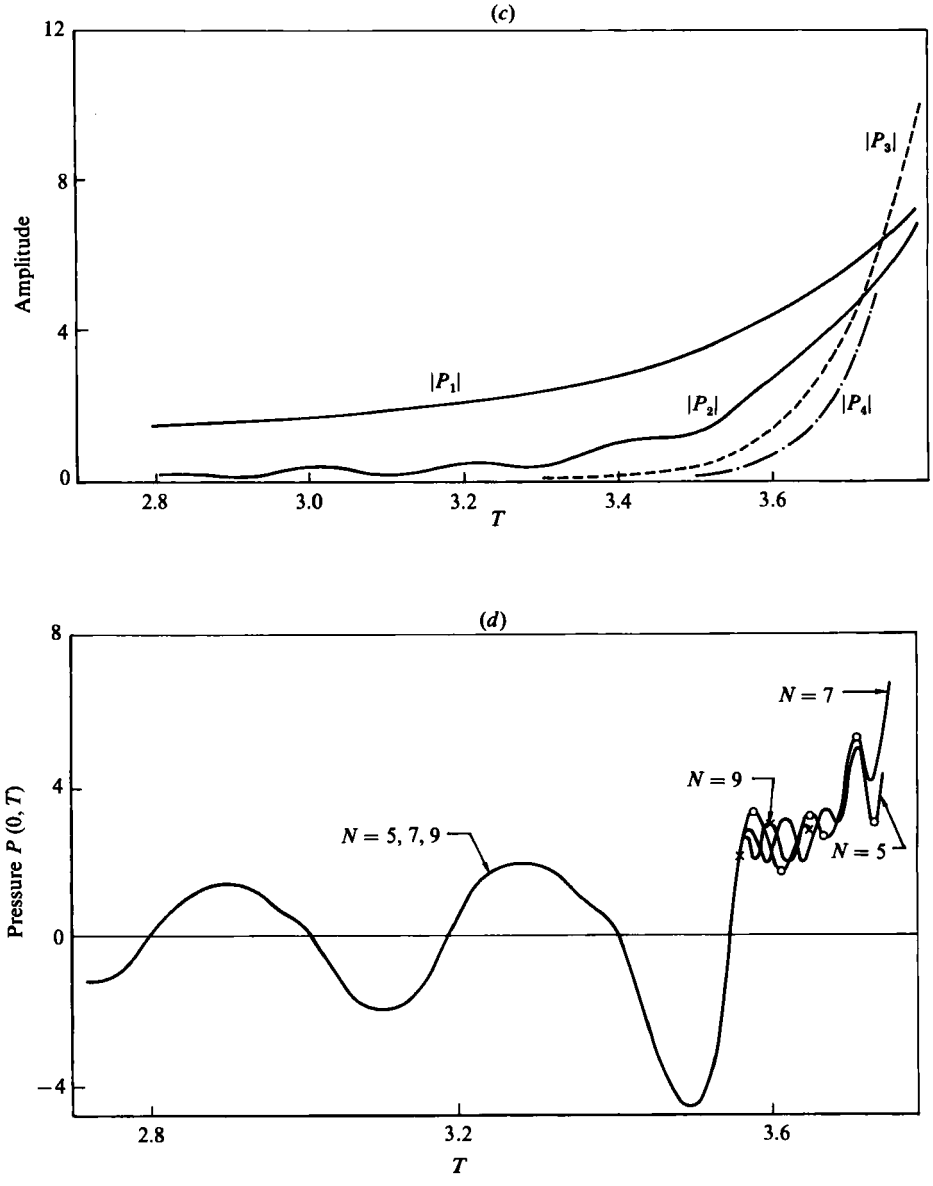

FIGURE 5. Computed spectral solution of the unsteady triple-deck problem (2.1*a–e*), for $\alpha = 4$. (*a*) Real part of the pressure fundamental P_1 (——) versus T. ◇, results for halved ΔT- and ΔY-steps with Y_∞ fixed; ×, Y_∞ doubled; ●, for N increased to 9. The bars indicate the theoretical high-frequency period according to (2.2). (*b*) Higher harmonics, compared with their theoretical periods. (*c*) The amplitudes versus T. (*d*) The calculated pressure for $N = 5, 7, 9$.

exponentially fast in the moving frame of $(X_1 - 2T_1)$, the correction pressure p_{11} can grow even faster in some non-parallel circumstances. A prime example is that of breakaway separation, where the incremental displacement $-\overline{A}(X_1)$ increases indefinitely like $X_1^{\frac{3}{2}}$ while $\overline{p} \to 0$ far downstream as $X_1 \to \infty$ [a similar event occurs upstream where $\overline{A}$, $\overline{p}$ grow like $|X_1|^{\frac{1}{6}}$, $|X_1|^{\frac{1}{2}}$ respectively]. The relative effect of the correction pressure above is then proportional to $\Omega^{-\frac{1}{2}} X_1^{\frac{3}{2}}$ and so becomes substantial at

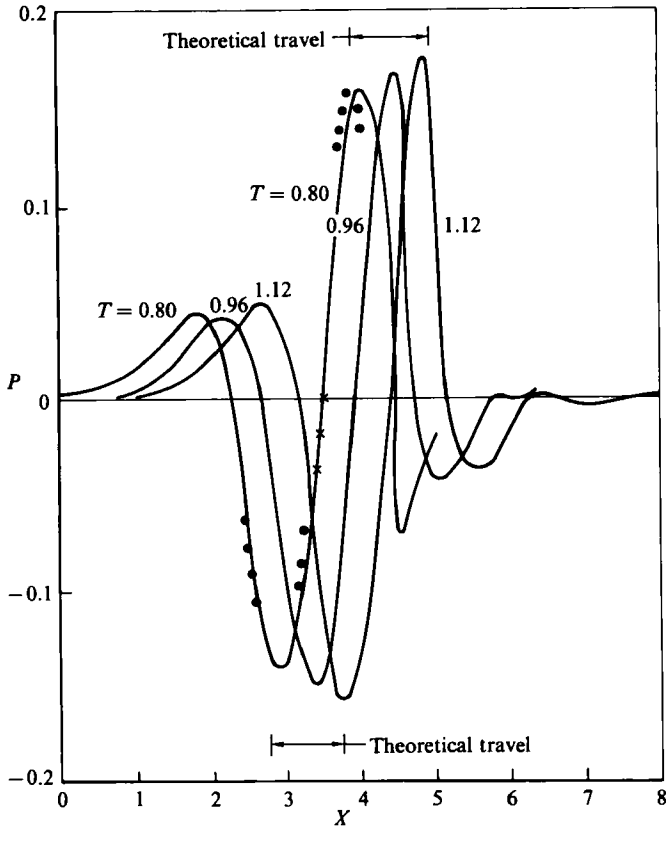

FIGURE 6. Finite-difference solution of the unsteady triple-deck problem, showing P vs. X at three times T. The effects of halving all the step sizes, with Y_∞ fixed, and of doubling Y_∞ with fixed step sizes, are denoted by ●, × respectively. Also shown (⟷) is the theoretical travel from $T = 0.80$ to 1.12 according to the high-frequency theory.

distances X_1 of order $\Omega^{\frac{1}{8}}$ downstream. A useful interpretation of this feature is in terms of the mean wall-shear stress, which here is

$$\text{mean-}\tau_w = \lambda(X_1) + \sqrt{2}|p_{01}|^2 \tag{6.2}$$

(cf. (6.1)). An initial disturbance $|p_{01}|$ made in the original reversed flow, say, where $\lambda(X_1) < 0$, travels downstream, growing and spreading, and induces a mean-flow re-attachment ultimately, but with the re-attachment point proceeding downstream at the group velocity. At distance $O(\Omega^{\frac{3}{8}})$ downstream, however, formally the correction-pressure influence can stop this travel, since that influence is controlled by the fixed $-X_1$ scale. Such an effect may well be connected with the turbulent re-attachment often observed experimentally downstream of a laminar separation: see also Smith (1985).

This paper first appeared as a United Technologies Research Center (East Hartford, CT, U.S.A.) Report UTRC-85-36, by the author. He wishes to thank Dr M. J. Werle (UTRC) and Dr R. E. Whitehead (ONR) for their interest, encouragement and partial support of this work, Dr J. Elgin and Dr D. Wood for helpful comments on equation (4.2), and Professor S. A. Maslowe and the referees for comments and for pointing out three references.

Appendix A. Further aspects of the nonlinear evolution equation

Several other relevant aspects of the evolution equation (2.20) studied in §§4 and 5 are discussed briefly below.

First, rather similar systems are considered by Bretherton & Spiegel (1983), Kuramoto (1978), Moon, Huerre & Redekopp (1982), Bullough, Fordy & Manakov (1982), Huppert & Moore (1976) and Kogelman & DiPrima (1970), but usually there are crucial differences from ours in the end conditions, e.g. spatial periodicity is assumed (see below), or in the signs or complexity of the coefficients, and associated with this, and as a referee notes, there are more unstable wavenumbers in the present system. Only Bretherton & Spiegel's work seems directly relevant, although there again spatial periodicity is imposed and the coefficients involved are still slightly different from those in (2.20). Bretherton & Spiegel note a useful analogy with water-layer motion, an analogy which we extend a little here. Taking $\gamma = 0$ in (5.1*a*, *b*), so that $B = R\exp(\mathrm{i}\theta)$ now, and with $R^2 = H\bar{h}$, $\partial\theta/\partial X_1 = H^{\frac{1}{2}}\bar{u}$, $X_1 = \Delta\bar{x}$, $T_2 = \Delta H^{-\frac{1}{2}}\bar{t}$, (5.1*a*, *b*) reduce to the equations

$$\frac{\partial\bar{u}}{\partial\bar{t}} + 2\bar{u}\frac{\partial\bar{u}}{\partial\bar{x}} = -\frac{\partial\bar{h}}{\partial\bar{x}}, \tag{A 1}$$

$$\frac{\partial\bar{h}}{\partial\bar{t}} + 2\frac{\partial}{\partial\bar{x}}(\bar{u}\bar{h}) = 0, \tag{A 2}$$

provided that the amplitude parameter H is large and the lengthscale Δ satisfies $H^{-\frac{1}{2}} \ll \Delta \ll H^{\frac{1}{2}}$. Here (A 1), (A 2) are exactly the inviscid shallow-water equations. The terms neglected in them are of relative orders $H^{-1}\Delta^{-2}$, $\Delta H^{-\frac{1}{2}}$ and stem from the highest derivative $\partial^2 R/\partial X_1^2$ and the growth term $-R/\sqrt{2}$ in (5.1*a*, *b*). For such a high-amplitude disturbance then, (A 1), (A 2) can be solved by characteristics, for increasing time $\bar{t}$. After a finite time $\bar{t}$, however, a 'shock' is inevitable, starting at some value of $\bar{x}$. Within the shock shorter time- and lengthscales, of orders H^{-1}, $H^{-\frac{1}{2}}$ respectively, therefore come into operation to smooth out the discontinuities of the (inviscid) solution: see also the next paragraph. With those scales a fuller set of equations applies, with only the above-noted growth term absent then. This set is equivalent to a standard cubic Schrödinger equation and admits stable solitary and modulated-carrier waves. At larger times the complete equation (2.20) is reinstated eventually, even for this extreme of a *large*-amplitude initial disturbance. At the other extreme, for *small* initial disturbances, the linearized form of (2.20) can be solved analytically by means of a Fourier transform in X_1, giving

$$2\pi p_{01}(X_1, T_2) = \exp\left[(1-\mathrm{i})\frac{T_2}{\sqrt{2}}\right]\int_{-\infty}^{\infty} Q(\omega)\exp\left[\mathrm{i}\omega X_1 - \mathrm{i}\omega^2 T_2\right]\mathrm{d}\omega, \tag{A 3}$$

where $Q(\omega)$ is the transform of the initial pressure disturbance. For an initial Gaussian distribution, for instance, we have the explicit solution

$$2\pi p_{01}(X_1, T_2) = \exp\left[(1-\mathrm{i})\frac{T_2}{\sqrt{2}} - \frac{\hat{b}^2 X_1^2}{1+4\mathrm{i}\hat{b}^2 T_2}\right]\Big/(1+4\mathrm{i}\hat{b}^2 T_2)^{\frac{1}{2}} \tag{A 4}$$

where $\hat{b}$ is a real constant. Hence the small disturbance grows in amplitude exponentially fast and spreads spatially (in a Gaussian form, from (A 3) or (A 4)) with $|X_1| \propto T_2^{\frac{1}{2}}$ (for waves) and T_2 (for amplitude dependence), at large times T_2. So again, at larger times, due to nonlinearity coming back into play, the full system (2.20) is reinstated. The above extremes confirm the need to address (2.20) computationally,

as was done in §4. A further comment concerning (A 4) is that, if $\hat{b}$ is purely imaginary, a singularity results at a finite time, $T_2 = \frac{1}{4}|\hat{b}|^{-2}$, but this comes from unrealistically strong wave-like conditions at large X_1.

If, next, spatial periodicity or spatial confinement is present, as in Bretherton & Spiegel (1983), then the growing plane-wave solution noted in (5.2) appears to be the most likely terminal form for large T_2. Its stability, for any T_2, as well as that of the unbounded form (5.3) to some extent, can be tested by examining a small disturbance $(\propto \hat{R}, \hat{\theta})$ for R, θ, governed by

$$-R\frac{\partial\hat{\theta}}{\partial T_2} - \hat{R}\left(\frac{\partial\theta}{\partial T_2}\right) - \hat{\alpha}^2\hat{R} - 3\mathrm{e}^{2\gamma T_2}R^2\hat{R} = 0, \tag{A 5}$$

$$\left(\gamma - \frac{1}{\sqrt{2}}\right)\hat{R} + \frac{\partial\hat{R}}{\partial T_2} - R\hat{\alpha}^2\hat{\theta} = 0, \tag{A 6}$$

from (5.1 a, b), where proportionality to $\exp(\mathrm{i}\hat{\alpha}X_1)$ is assumed. From (A 5), (A 6) and with θ given in (5.2), the disturbance $\hat{R}(T_2)$ is controlled by the Bessel equation

$$s^2\frac{\partial^2\hat{R}}{\partial s^2} + s\frac{\partial\hat{R}}{\partial s} + 2(\hat{\alpha}^4 + 2\hat{\alpha}^2R^2s^2)\,\hat{R} = 0 \tag{A 7}$$

with $s \equiv \exp(\gamma T_2)$. The corresponding Bessel functions show that there is no growth in the disturbance $\hat{R}$ for any wavenumber $\hat{\alpha}$ as time, and hence s, increases. This is tantamount to the conclusion that the Benjamin–Feir (1967) secondary-instability mechanism does not occur in the present two-dimensional motions, a conclusion which can be verified for the more general case (5.3) also. On the other hand, a factor $\exp(\gamma T_2)$ has been absorbed into (5.1 a, b). Thus although $\hat{R}$ decays like $s^{-\frac{1}{2}}$ according to (A 7), i.e. like $\exp(-\frac{1}{2}\gamma T_2)$, the actual disturbance $\exp(\gamma T_2)\hat{R}$ grows like $\exp(\frac{1}{2}\gamma T_2)$. This growth is small relative to the growth of the basic solution (5.2), but it is growth nevertheless and it could account for the extra oscillations sometimes observed in the numerical solutions (§4) at larger times, not dissimilar to those found by Bretherton & Spiegel (1983) and perhaps of a somewhat random nature. It can be shown analytically, however, that more sizeable (nonlinear) dips of amplitude $O(\exp(\gamma T_2))$ and X_1 scale of $O(\exp(-\gamma T_2))$ cannot persist for large times T_2 in the spatially periodic case.

Appendix B. Computational solutions of the unsteady triple-deck flow

Numerical solutions of the original unsteady triple-deck problem (2.1 a–e) were obtained in two different ways, as mentioned in §6 and in Smith (1984) and summarized below.

Method (i) is a spectral approach to (2.1 a–e), in which spatial periodicity over a prescribed length $2\pi/\alpha$ is assumed. The flow variables are expressed as the Fourier series

$$[U, \Psi, P, A] = \sum_{-\infty}^{\infty} [u_n(Y,T), \psi_n(Y,T), p_n(T), a_n(T)]\exp(\mathrm{i}n\alpha X) \tag{B 1}$$

with unknown coefficients u_n, ψ_n, p_n, a_n. Formal substitution of (B 1) into (2.1 a, b) therefore yields coupled differential equations in Y, T for u_n, ψ_n with the coefficients p_n, a_n determined by the boundary and matching conditions (2.1 c–e). This coupled system is truncated at N terms and solved iteratively at each time level. The techniques used here are those of Smith, Papageorgiou & Elliott (1984), the main difference being the determination of the mean flow to satisfy the displaced shear

condition $u_0 \sim Y + a_0$ as $Y \to \infty$. Time-marching is performed in the Crank–Nicholson manner as in method (ii) below. Typically (see also figure 5) the value of N is set at 7 and a Y-grid of 101×0.1 is taken, transformed as in (ii) below, with a timestep of 0.001 and an overall tolerance per timestep of 10^{-6} in the maximum pressure difference. Results are shown in figure 5 for an initial disturbance given by $u_0 = Y$ and, for $n \geqslant 1$,

$$[u_n, p_n] = \frac{(1+\mathrm{i})[(2Y - Y^2)\,\mathrm{e}^{-Y}, 1]}{(n+1)^5} \tag{B2}$$

at $T = 0$, with the value $\alpha = 4$ which is nominally supercritical. As was remarked in §6, the temporal evolution of a representative property of the fundamental agrees well with the linear and weakly nonlinear theory of high frequencies for stage 1. This is until stronger nonlinearity comes into force at later times, and then the calculations become more difficult and are rather sensitive to the grid sizes and the series truncation adopted, although the results then are quite possibly in line with the features expected for the subsequent stage 2, as mentioned near the end of §6.

In method (ii) we take finite differencing in X, Y, T of second-order accuracy, and march forward in time T, solving at each time level by sweeping the (X, Y)-plane M times to obtain convergence. The differencing and notation used are similar to those in §5 with respect to the X- and T-dependence, while for the Y-dependence we choose a box technique. The momentum equation (2.1*b*) for instance is thereby represented as

$$2[U^{(\mathrm{a})}_{i-\frac{1}{2},j-\frac{1}{2}} - U^{(\mathrm{o})}_{i-\frac{1}{2},j-\frac{1}{2}}]/\Delta T + \frac{[(U_{i,j-\frac{1}{2}})^2 - (U_{i-1,j-\frac{1}{2}})^2]^{(\mathrm{a})}}{2\Delta X} - \frac{[\psi_{i,j-\frac{1}{2}} - \psi_{i-1,j-\frac{1}{2}}]^{(\mathrm{a})}[\tau_{i-\frac{1}{2},j-\frac{1}{2}}]^{(\mathrm{a})}}{\Delta X}$$
$$= -\frac{[P_i - P_{i-1}]^{(\mathrm{a})}}{\Delta X} + \frac{[\tau_{i-\frac{1}{2},j} - \tau_{i-\frac{1}{2},j-1}]^{(\mathrm{a})}}{\Delta Y}, \tag{B3}$$

where ΔX, ΔY, ΔT are the steplengths, the subscripts i, j refer to the X- and Y-directions in turn, $\tau \equiv \partial U/\partial Y$, and the values at $i-\frac{1}{2}$, $j-\frac{1}{2}$ denote the means of the values at i, $i-1$ and j, $j-1$ respectively. Thus at each half-time level$^{(\mathrm{a})}$ the computational task is analogous to that for steady subsonic-flow problems and so we adapt the approach of Smith & Merkin (1982), where more details are available. Local updating of the pressure–displacement relation (2.1*e*) is imposed at each X-station in the Veldman–Davis fashion (Veldman & Dijkstra 1980; Davis 1984), with Newton iteration to handle the nonlinearity, while to accommodate the far-field conditions imposed, (2.1*d*) and $(U, \Psi, P, A) \to (Y, \frac{1}{2}Y^2, 0, 0)$ as $|X| \to \infty$, both the X- and Y-coordinates are transformed. Windward differencing in X has also been included to allow for flow reversals. Once the solution at the current half-time level$^{(\mathrm{a})}$ has converged, after M sweeps, the solution at the time level$^{(\mathrm{n})}$ follows from $(\,)^{(\mathrm{n})} = 2(\,)^{(\mathrm{a})} - (\,)^{(\mathrm{o})}$, schematically, and the time is then stepped forward to the next level. Typically (see also figure 6) we took steplengths 0.004, $\pi/200$, 0.1 in T and the transformed X, Y, respectively, while 2–3 Newton iterates were required per X-station and M was usually about 3–4, to satisfy a tolerance of 10^{-6} on the maximum difference in pressure per sweep of the flow field. The overall accuracy, which is no more than graphical, has also been checked against calculations done in the original untransformed coordinates X, Y. A sample result is shown in figure 6. Some preliminary results for flow due to maintained oscillations of a hump were given by Smith (1984) and in a report by the author to the Science and Engineering Research Council, U.K., in 1981. In figure 6, by contrast, the hump given by $Y = [2/(1+X^2)]\sin(\Omega T)$, with $\Omega = 4$, is maintained only for times T up to 0.1 and then abruptly switched off. This effectively sets up an initial-value problem for the subsequent times. It is found that

a wave packet propagates downstream, as described in §6, its features tying in reasonably well with the high-frequency theory. At later times a more erratic response emerges. Similar downstream-travelling behaviour could also be observed in the earlier results for maintained oscillations of a hump.

REFERENCES

BENJAMIN, T. B. & FEIR, J. E. 1967 *J. Fluid Mech.* **27**, 417.

BENNEY, D. J. & MASLOWE, S. A. 1975 *Stud. Appl. Math.* **54**, 181.

BRETHERTON, C. S. & SPIEGEL, E. A. 1983 *Phys. Lett.* **96 A**, 152.

BULLOUGH, R. K., FORDY, A. P. & MANAKOV, S. V. 1982 *Phys. Lett.* **91 A**, 98.

CRIMINALE, W. O. & KOVASZNAY, L. S. G. 1962 *J. Fluid Mech.* **14**, 59.

DAVIS, R. T. 1984 *AIAA Paper No.* 84-1614 (presented June 1984, Snowmass, Colorado).

DUCK, P. W. 1985 *J. Fluid Mech.* **160**, 465.

FASEL, H. 1984 In *Proc. Symp. on Turb. & Chaotic Phen. in Fluids, Kyoto, Japan* (ed. T. Tatsumi). Elsevier.

GAJJAR, J. & SMITH, F. T. 1985 *J. Fluid Mech.* **157**, 53.

GASTER, M. 1984 In *Proc. Symp. on Turb. & Chaotic Phen. in Fluids, Kyoto, Japan* (ed. T. Tatsumi). Elsevier. See also *Transition and Turbulence* (ed. R. E. Meyer), 1981, p. 95. Academic.

GATSKI, T. B. 1983 *NASA Tech. Paper* 2245 (see also *Proc. R. Soc. Lond.* A **397**, 1985, 397).

HASTINGS, S. & MCLEOD, J. 1978 *MRC Rep.* 1861.

HERBERT, T. 1984 *AIAA Paper No.* 84-0009 (presented January 1984, Reno, Nevada).

HOCKING, L. M. & STEWARTSON, K. 1972 *Proc. R. Soc. Lond.* A **326**, 289.

HUPPERT, H. E. & MOORE, D. R. 1976 *J. Fluid Mech.* **78**, 821.

KLEBANOFF, P. S., TIDSTROM, D. K. & SARGENT, L. M. 1962 *J. Fluid Mech.* **12**, 1.

KOGELMAN, S. & DIPRIMA, R. C. 1970 *Phys. Fluids* **13**, 1.

KURAMOTO, Y. 1978 *Prog. Theor. Phys. Suppl.* No. 64, p. 346.

LANGE, C. G. & NEWELL, A. C. 1974 *SIAM J. Appl. Maths* **27**, 441.

MASLOWE, S. A. 1981 *Hydrodynamic Instabilities and the Transition to Turbulence* (ed. H. L. Swinney & J. R. Gollub), Chap. 7. Springer.

MESSITER, A. F. 1983 *Trans. ASME* **50**, 1104.

MOON, H. T., HUERRE, P. & REDEKOPP, L. G. 1982 *Phys. Rev. Lett.* **49**, 458.

NOZAKI, K. & BEKKI, N. 1983 *Phys. Rev. Lett.* **51**, 2171.

RYZHOV, O. S. & ZHUK, V. I. 1980 *J. Méc.* **19**, 561.

SARIC, W. S., KOZLOV, V. V. & LEVCHENKO, V. YA. 1984 *AIAA Paper No.* 84-0007 (presented January 1984, Reno, Nevada).

SMITH, F. T. 1979*a* *Proc. R. Soc. Lond.* A **366**, 91.

SMITH, F. T. 1979*b* *Proc. R. Soc. Lond.* A **368**, 573 (see also *Proc. R. Soc. Lond.* A **371**, 439).

SMITH, F. T. 1984 *AIAA Paper No.* 84-1582 (presented June 1984, Snowmass, Colorado).

SMITH, F. T. 1985 In *Proc. Symp. on Stability of Spatially-Varying and Time-Dependent Flows, NASA Langley Res. Center, Hampton, VA, August* 19–20, 1985. Also *Utd. Tech. Res. Cent. Rep.* UTRC-85-55.

SMITH, F. T. 1986 *Ann. Rev. Fluid Mech.* **18**, 197.

SMITH, F. T. & BODONYI, R. J. 1985 *Aeronaut. J. paper no.* 1313, June/July, p. 205.

SMITH, F. T. & BURGGRAF, O. R. 1985 *Proc. R. Soc. Lond.* A **399**, 25.

SMITH, F. T. & MERKIN, J. H. 1982 *Computers & Fluids* **10**, 7.

SMITH, F. T., PAPAGEORGIOU, D. & ELLIOTT, J. W. 1984 *J. Fluid Mech.* **146**, 313.

STEWARTSON, K. & STUART, J. T. 1971 *J. Fluid Mech.* **48**, 529.

STUART, J. T. & DIPRIMA, R. C. 1978 *Proc. R. Soc. Lond.* A **362**, 27.

TUTTY, O. R. & COWLEY, S. J. 1986 *J. Fluid Mech.* (to appear).

VELDMAN, A. E. P. & DIJKSTRA, D. 1980 In *Proc. 7th Intl Conf. Num. maths. Fluid Dyn., Stanford, CA.*

WALKER, J. D. A. & ABBOTT, D. E. 1977 In *Turbulence in Internal Flows* (ed. S. N. B. Murthy), p. 131. Hemisphere.

WALKER, J. D. A. & SCHARNHORST, R. K. 1977 In *Recent Advances in Engineering Science* (ed. G. C. Sih), p. 541. University Press, Bethlehem, Penn.

WYGNANSKI, I., SOKOLOV, M. & FRIEDMAN, D. 1976 *J. Fluid Mech.* **78**, 785.